Numerical Methods in Civil Engineering

Journal Homepage: https://nmce.kntu.ac.ir/

Buckling analysis of axially functionally graded carbon nanotubes-reinforced columns using the meshless method

Hanie Elahihamezanlui[*], Majid Kazemi [**] and Mohammad Hosein Ghadiri Rad[***]

ARTICLE INFO

RESEARCH PAPER

Article history:
Received:
December 2021.
Revised:
June 2022.
Accepted:
June 2022.

Keywords:
Carbon Nanotubes,
Meshless Method,
Buckling of Column,
Functionally Graded Materials
Composite Materials,

Abstract:

The spread of different material processing technologies has led to novel methods developed for reinforcing structural members. One of these approaches is to add carbon nanotubes (CNTs) with different distributions through the matrix phase of composite materials to improve their properties. Due to their superior properties such as lightweight and high values of elastic modulus, elastic strain, and failure strain, CNTs can be used to reinforce structures and elements. The present paper aims to investigate the effect of adding CNTs as reinforcement of matrix on the buckling capacity of columns by applying the meshless local Petrov-Galerkin (MLPG) method for buckling analysis. Since the MLPG method uses some scattered nodes through the domain and boundaries for discretization (rather than the meshing), the functionally graded (FG) variation of material properties can be conveniently modeled under the influence of reinforcing elements (CNTs). Four types of volume fraction exponent functions are considered for modeling the FG variation of the CNT volume fraction to examine the effect of CNTs distribution on the buckling capacity of the column and determine the most optimal distribution of CNTs. Effective mechanical properties of the CNT-reinforced column are estimated based on the extended rule of mixture. Results show that reinforcing the polymer matrix with a low volume fraction of CNTs with appropriate distribution can significantly increase its buckling capacity. Using the obtained results, one can determine the best distribution pattern of CNTs in the longitudinal direction of the column at various boundary conditions.

1. Introduction

The stability of columns is a critical issue in the engineering design of structures. The stability of prismatic columns made of homogeneous materials can be investigated analytically [1,2]. However, for the optimal design of buildings and bridges, different approaches such as non-prismatic columns (change in the column cross-section) and the reinforcement of columns in weak points (change in the material properties) have been suggested to increase the load-bearing capacity of columns [3]. In both methods, the flexural stiffness varies through the column length, and except for some particular cases, it is extremely difficult to provide an analytical approach for this type of column [4,5]. In order to determine the buckling capacity of columns with variable flexural stiffness, various techniques such as finite-difference [6], polynomial series [7], boundary element [8], integral-based relationships [9,10], finite element [11,12], and meshless [13,14] methods have been presented.

Functionally graded materials are new types of materials with favorable resistance that can manage the distribution of material properties [15]. Recently, functionally graded materials (FGMs) have been widely used in engineering applications and industries. There are some papers on stability analysis of FG members. For instance, an improved approach based on the power series expansions was proposed by Soltani and Asgarian [16] to exactly evaluate the static and buckling stiffness matrices for the linear stability analysis of axially functionally graded (AFG) Timoshenko beams with variable cross-section and fixed-free boundary condition. Soltani et al. [17] developed the finite difference method for buckling analysis of tapered Timoshenko beam made of axially functionally graded

* *Master, Department of Civil Engineering, Quchan University of Technology, Quchan, Iran.*
** *Assistant Professor, Department of Civil Engineering, Quchan University of Technology, Quchan, Iran.*
*** *Corresponding author. Assistant Professor, Department of Civil Engineering, Quchan University of Technology, Quchan, Iran. E-mail: hosein_ghadiri@qiet.ac.ir*

https://doi.org/10.52547/NMCE.2022.374

material. In another work Soltani [18] developed an efficient finite element model with two degrees of freedom per node for buckling analysis of AFG tapered Timoshenko beams resting on Winkler elastic foundation. Soltani and Asgarian [19] studied the lateral-torsional stability of axially functionally graded beams with tapered bi-symmetric I-section subjected to various boundary conditions. The lateral-torsional buckling behavior of FG non-local beams with a tapered I-section and the flexural-torsional stability of functionally graded (FG) nonlocal thin-walled beam-columns with a tapered I-section were investigated by Soltani et al. [20, 21].

In the past few years, polymer matrices reinforced by nanomaterials because of their excellent mechanical and thermal properties, have attracted many researchers' attention [22]. Among nano-reinforcements materials, carbon-type ones like graphene [23] and CNTs [24] have been the best contribution in improving mechanical and thermal properties. An overview of recently published papers shows that the CNTs have been successfully utilized as the reinforcement of different matrices [25,26]. For instance, Zhang et al. [27] studied the effect of column reinforcement by CNTs on the force-displacement curve in an experimental study. Han and Elliott [28] estimated the elastic and shear moduli of CNT-reinforced composite materials based on the theorem of minimum strain-energy and compared the results with those obtained from the rule of mixture. Yas and Samadi [29] worked on the buckling analysis of the CNT reinforced Timoshenko beams resting on an elastic foundation. The free vibration analysis of thick composite plates reinforced by FG-CNTs along the plate thickness was studied by Lei et al. [30]. Li et al. [31] reviewed studies conducted on the effect of reinforcing cementitious composites by CNTs on the elastic modulus, porosity, fracture, and other mechanical properties of cement-based composite materials. Mirzaei and Kiani [32] analyzed the free vibration of cylindrical panels reinforced by CNTs. Arani and Kolahchi [33] studied the buckling behavior of embedded concrete columns armed with carbon nanotubes based on the energy method, and Hamilton's principle. Different effects of the distribution of CNTs along the thickness on the vibration of double-curved panels and circular shells were studied by Wang et al. [34]. Karami et al. [35] studied the buckling behavior of composite curved beams reinforced by functionally graded CNTs using the non-local theory that considers dependency between structural dimensions in small scales. Civalek and Jalaei [36] studied the shear buckling behavior of FG-CNTR skew plates with opposing boundary conditions. Liew et al. [37] conducted a brief review on studies on the composite materials reinforced by CNTs of different distributions.

In the general finite element method (FEM), the mechanical properties of each element are constant. Therefore, there are some drawbacks in applying this method to analyze FG nanomaterials-reinforced polymer matrices, in which the material properties gradually varied in a direction. Thus, in the FEM, the variation of properties must be applied manually by the user, which is a time-consuming process. Hence, several meshless methods have been proposed in recent years to analyze the FGM structures. Ghayoumizadeh et al. [38] investigated the wave propagation of displacement and stresses through the CNT-reinforced composite materials using the meshless method. Ghoohestani et al. [39] studied the dynamic behavior of structures made of CNT-reinforced multi-layer composite materials under impact loading. Rad et al. [40] evaluated the geometrically nonlinear dynamic behavior of hollow cylindrical structures made of FGM with variable properties along the radius direction using the MLPG method. Hosseini and Zhang [41] utilized the meshless finite difference method to analyze the time history of FG graphene platelet-reinforced (FG-GPLTR) cylindrical structures with variable properties in the radial direction. They also examined the thermo-elastic behavior of FG-GPLTR multi-layer structures using the meshless method in another study [42]. All of the above-mentioned articles are in the field of functionally graded and multilayer GPLs and CNTs reinforced plates and shells in which the nanoparticle content gradually varies in the thickness direction. Since continuous changes of material properties in thickness direction of plates and shells cause a change in the flexural rigidity parameter, the finite element method can be easily applied for analysis of these problems. In the present study, for the first time, the MLPG method is developed for the buckling analysis of axially functionally graded (AFG) CNTs-reinforced columns in which the CNT volume fraction gradually changes in the longitudinal direction of column (problem domain). As previously described, applying of the MLPG method for analysis of AFG reinforced columns is a less time-consuming method compared with the finite element method. Analytical results show that the critical buckling load of the column may be enhanced significantly by strengthening the matrix with the CNTs. Therefore, it is recommended to consider these materials for special structural members that require lightweight and optimal design. Moreover, numerical results demonstrate that the buckling capacity of CNTR composite columns is highly dependent on the CNT distribution pattern.

2. Effective mechanical properties

A column with 4m length is considered, as shown in Figure 1. Four different nonlinear functions are considered in this paper to model the CNTs distribution through the length of the column. The volume fraction of the CNTs (V_{CNT}) for various distribution patterns are defined as follows [43].

Type 1:

$$V_{CNT}(x)=2\times V_{CNT}^{*}\left(\frac{x}{L}\right)^{\alpha} \quad (1)$$

Type 2:

$$V_{CNT}(x)=2\times V_{CNT}^{*}\left(\frac{L-x}{L}\right)^{\alpha} \quad (2)$$

Type 3:

$$V_{CNT}(x)=2\times V_{CNT}^{*}\left|\frac{2(x-x_m)}{L}\right|^{\alpha} \quad (3)$$

Type 4:

$$V_{CNT}(x)=2\times V_{CNT}^{*}\left|\frac{2(L-(x-x_m))}{L}\right|^{\alpha} \quad (4)$$

where α is the volume fraction exponent, and other parameters are calculated by the following equations [43]:

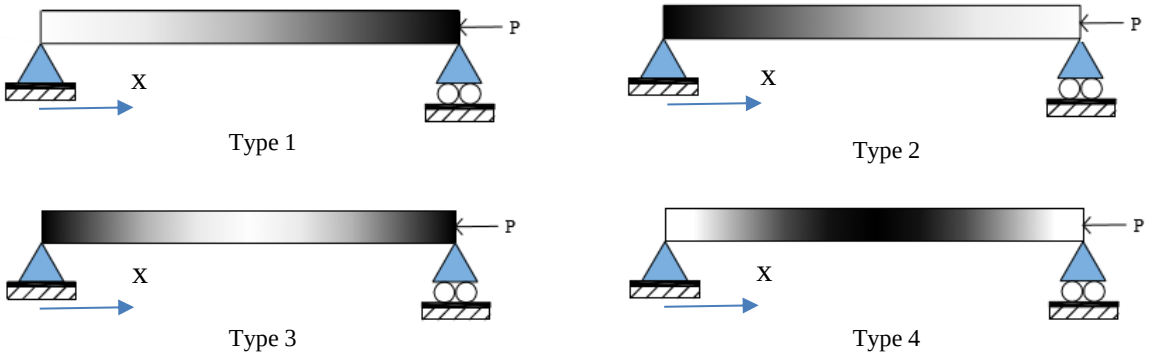

Fig. 1: Different patterns of CNTs distribution through the column length

$$x_m=\frac{L}{2} \quad (5)$$

$$V_{CNT}^{*}=\frac{\rho_m}{w_{CNT}+(\frac{\rho_{CNT}}{w_{CNT}})-\rho_{CNT}} \quad (6)$$

where w_{CNT} and ρ_{CNT} are the weight fraction and density (mass per volume) of CNTs, and ρ_m is the matrix density. For more simplicity, the extended rule of mixtures is employed to estimate the effective elastic modulus of CNTR column, which is expressed as follows [43]:

$$E(x)=\eta_1 V_{CNT}(x)\,E_{CNT}+V_m(x)\,E_m \quad (7)$$

where η_1 is the efficiency parameter, E_{CNT} and E_m are the elastic modulus of CNT and matrix, respectively, and V_m is the matrix volume fraction. The CNT distribution pattern along the columns length for all types of functions is shown in Figure 1. In this figure, the darker color represents more CNT contents.

The following relationship is established between matrix and CNT volume fractions.

$$V_m(x)=1-V_{CNT}(x) \quad (8)$$

It worth mentioning that the single-walled carbon nanotubes (SWCNTs) are utilized as column reinforcements in the present study. The properties of the matrix and CNTs are demonstrated in Table 1. In this table the matrix phase is considered as: poly{(m-phenylenevinylene)-co-[(2,5-dioctoxy-p phenylene) vinylene]}, and geometry properties of SWCNT is (L = 9.26 nm, R = 0.68 nm, h = 0.067 nm) [44].

Table 1: Mechanical properties of matrix and CNT [44]

Matrix	CNT
$E_m=2\,\text{GPa}$	$E_{CNT}=5.64\,\text{TPa}$
$\rho_m=1150\,\frac{\text{kg}}{\text{m}^3}$	$\rho_{CNT}=1400\,\frac{\text{kg}}{\text{m}^3}$
$\nu_m=0.34$	$\eta_1=0.149$

Figure 2 represents the variation of elastic modulus along the column length for all functions with a constant volume fraction exponent $\alpha = 0.5$ and various values of V_{CNT}^{*}. Figure 3 illustrates the variation of elastic modulus along the column length for different values of volume fraction exponent.

3. MLPG method for buckling analysis of the column

Consider an FG-CNTR simply supported column with functionally graded elasticity modulus 'E(x)' and constant moment of inertia 'I' subjected to an axial load 'P'. From the force and moment equilibrium of a differential element of the column we have:

$$M(x)-PW+Cx+D=0 \quad (9)$$

where the values of C and D depend on the boundary conditions. The curvature of the beam (which can be considered as pseudo strain) is related to the moment

(pseudo stress) by $M(x) = EIW''$. Substituting this result into Equation (9) and then differentiating the obtained equation twice with respect to '*x*', the governing fourth order differential equation of buckling for all boundary conditions can be obtained as follows:

$$E(x)I\frac{d^4W}{dx^4} - PW'' = 0 \tag{10}$$

where '*W*' is the lateral displacement of the column. At each end of the column (*x=0* and *x=L*) two boundary conditions should be defined. The boundary conditions are on deflections '*W*', slope '*θ=dW/dx*', moment '*M=EI(d²W/dx²)*', and shear force '*V= -EI(d³W/dx³)*' . Instead of solving this differential equation, the weak form of Equation (10) is minimized over a local subdomain of each node 'Ω' [45]:

$$\int_{\Omega}\left(\frac{d^2}{dx^2}\left(E(x)I\frac{d^2W}{dx^2}\right) - PW''\right)\psi\, d\Omega = 0 \tag{11}$$

Where 'ψ' is the weight function. By integration of parts twice, Equation (11) can be rewritten as follows:

$$\begin{aligned}&\int_{\Omega}\left(E(x)I\frac{d^2W}{dx^2}\frac{d^2\psi}{dx^2}\right)d\Omega + \left[n_x\frac{d}{dx}\left(E(x)I\frac{d^2W}{dx^2}\right)\psi\right]_{\Gamma}\\ &-\left[n_x\left(E(x)I\frac{d^2W}{dx^2}\right)\frac{d\psi}{dx}\right]_{\Gamma} - \int_{\Omega}\left(P\frac{d^2W}{dx^2}\right)\psi\, d\Omega\\ &+\alpha_w\left[\left(W-\bar{W}\right)\psi\right]_{\Gamma_w} + \alpha_\theta\left[\left(\frac{dW}{dx}-\bar{\theta}\right)\psi\right]_{\Gamma_\theta} = 0\end{aligned} \tag{12}$$

where α_w and α_θ are penalty factors, which are usually very large numbers to enforce the deflection and slope boundary conditions. n_x=-1 at the left boundary point and n_x=+1 at the right boundary point.

The weight function ψ is usually a simple function that can be differentiated easily. By applying the shape functions, the displacement field can be expressed with respect to the nodal displacements and rotations as follows.

$$W = \sum_{i=1}^{N}\left(\phi_i^w W_i + \phi_i^\theta \theta_i\right) \tag{13}$$

where ϕ_i^w and ϕ_i^θ are the shape functions of the *i*th node created using all nodes in the support domain, W_i and θ_i are the displacement and rotation at node i . It should be mentioned that the present study utilizes the radial basis function (RBF) as the shape function that will be detailed in the next section. The weight function can also be estimated as in reference [46] as

$$\psi = \mu_i^w \chi_i^w + \mu_i^\theta \chi_i^\theta \tag{14}$$

where μ_i^w and μ_i^θ are arbitrary constants. In the current study, the power weight functions are considered as the components of the test functions [47]:

$$\chi_i^w = \begin{cases}\left[1-\left(\frac{d_i}{s_0}\right)^2\right]^4 & 0 \le d_i \le s_0\\ 0 & d_i > s_0\end{cases} \tag{15}$$

$$\chi_i^\theta = \frac{d\chi_i^w}{dx} \tag{16}$$

In these equations '$d_i = \|x - x_i\|$' is the distance to the node 'i' and s_0 determines the extent of the test functions. Substituting Equation (13) into Equation (12) yields to:

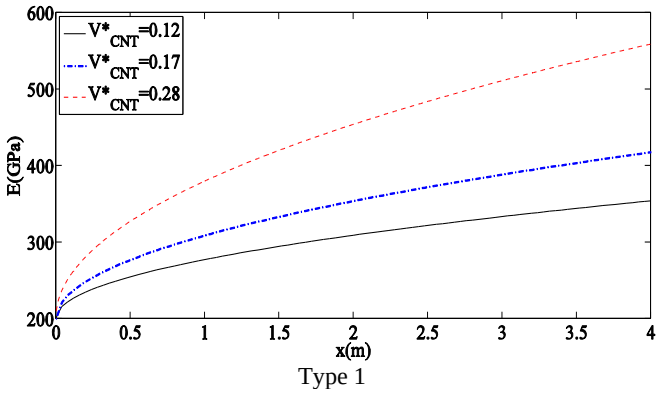

Type 1

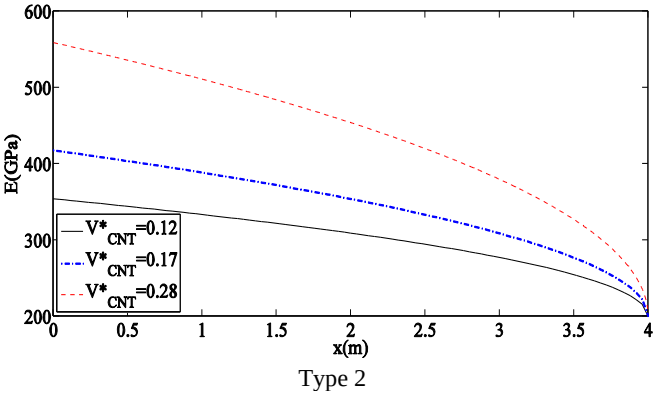

Type 2

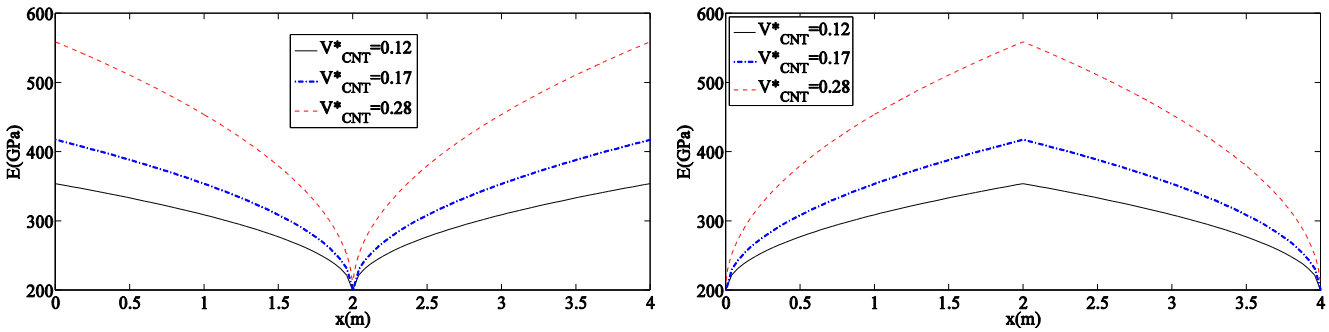

Type 3 Type 4

Fig. 2: Elastic modulus variation in the column length for α = 0.5 and different values of V_{CNT}^{*}

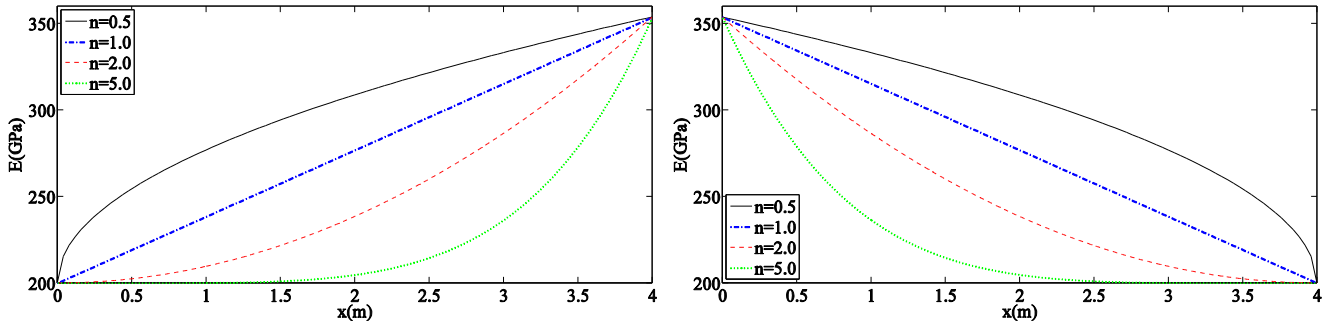

Type 1 Type 2

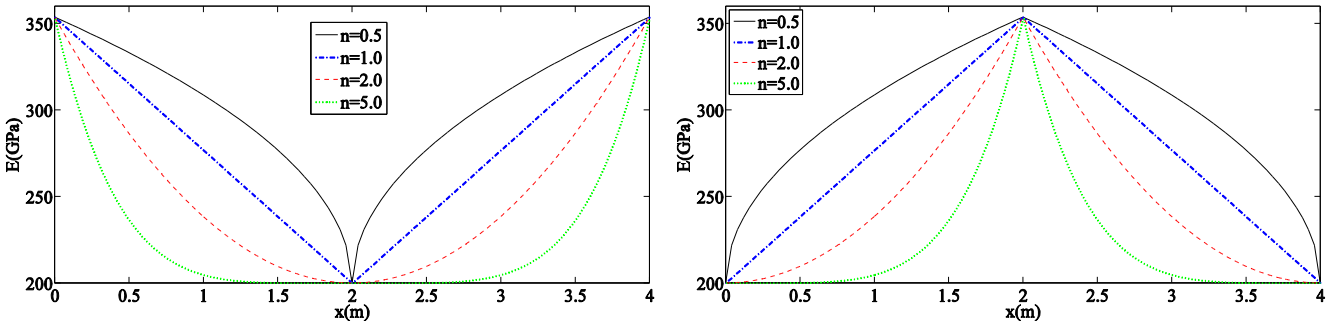

Type 3 Type 4

Fig. 3: Elastic modulus variation in the column length for $V_{CNT}^{*} = 0.12$ and different values of α

Table 2: Different types of RBFs [10]

No.	RBF	Formula	Shape parameters
1	Multi-quadric (MQ)	$R_i(x) = \left[(x-x_i)^2 + c^2\right]^q$	c, q
2	Gaussian (EXP)	$R_i(x) = \exp\left[-c(x-x_i)^2\right]$	c
3	Thin plat spline (TPS)	$R_i(x) = (x-x_i)^\eta$	η
4	Logarithmic	$R_i(x) = (x-x_i)^\eta \log(x-x_i)$	η

$$\left([K]+P[K_P]\right)\{d\}=0 \qquad (17)$$

where $\{d\}$ is the nodal displacement vector, $[K]$ is the stiffness matrix and $[K_P]$ is the geometric stiffness matrix [46].

$$\{d\}^{\mathrm{T}} = \{W_1 \quad \theta_1 \quad W_2 \quad \theta_2 \quad \mathrm{L} \quad W_N \quad \theta_N\} \tag{18}$$

$$k_{ij}^{node} = \mathrm{I}\begin{bmatrix} \int_\Omega \left(\mathrm{E}(x)\frac{d^2\chi_i^w}{dx^2}\frac{d^2\phi_j^w}{dx^2}\right)d\Omega & \int_\Omega \left(\mathrm{E}(x)\frac{d^2\chi_i^w}{dx^2}\frac{d^2\phi_j^\theta}{dx^2}\right)d\Omega \\ \int_\Omega \left(\mathrm{E}(x)\frac{d^2\chi_i^\theta}{dx^2}\frac{d^2\phi_j^w}{dx^2}\right)d\Omega & \int_\Omega \left(\mathrm{E}(x)\frac{d^2\chi_i^\theta}{dx^2}\frac{d^2\phi_j^\theta}{dx^2}\right)d\Omega \end{bmatrix}$$

$$+n_x\mathrm{I}\begin{bmatrix} \mathrm{E}(x)\chi_i^w\frac{d^3\phi_j^w}{dx^3} & \mathrm{E}(x)\chi_i^w\frac{d^3\phi_j^\theta}{dx^3} \\ \mathrm{E}(x)\chi_i^\theta\frac{d^3\phi_j^w}{dx^3} & \mathrm{E}(x)\chi_i^\theta\frac{d^3\phi_j^\theta}{dx^3} \end{bmatrix}_{\Gamma_1} \tag{19}$$

$$-n_x\mathrm{I}\begin{bmatrix} \mathrm{E}(x)\frac{d\chi_i^w}{dx}\frac{d^2\phi_j^w}{dx^2} & \mathrm{E}(x)\frac{d\chi_i^w}{dx}\frac{d^2\phi_j^\theta}{dx^2} \\ \mathrm{E}(x)\frac{d\chi_i^\theta}{dx}\frac{d^2\phi_j^w}{dx^2} & \mathrm{E}(x)\frac{d\chi_i^\theta}{dx}\frac{d^2\phi_j^\theta}{dx^2} \end{bmatrix}_{\Gamma_1}$$

$$k_{ij}^{bdry} = \alpha_w\begin{bmatrix} \chi_i^w\phi_j^w & \chi_i^w\phi_j^\theta \\ \chi_i^\theta\phi_j^w & \chi_i^\theta\phi_j^\theta \end{bmatrix}_{\Gamma_{sw}}$$

$$+n_x\mathrm{I}\begin{bmatrix} \mathrm{E}(x)\chi_i^w\frac{d^3\phi_j^w}{dx^3} & \mathrm{E}(x)\chi_i^w\frac{d^3\phi_j^\theta}{dx^3} \\ \mathrm{E}(x)\chi_i^\theta\frac{d^3\phi_j^w}{dx^3} & \mathrm{E}(x)\chi_i^\theta\frac{d^3\phi_j^\theta}{dx^3} \end{bmatrix}_{\Gamma_{sw}}$$

$$+\alpha_\theta\begin{bmatrix} \frac{d\chi_i^w}{dx}\frac{d\phi_j^w}{dx} & \frac{d\chi_i^w}{dx}\frac{d\phi_j^\theta}{dx} \\ \frac{d\chi_i^\theta}{dx}\frac{d\phi_j^w}{dx} & \frac{d\chi_i^\theta}{dx}\frac{d\phi_j^\theta}{dx} \end{bmatrix}_{\Gamma_{s\theta}} \tag{20}$$

$$-n_x\mathrm{I}\begin{bmatrix} \mathrm{E}(x)\frac{d\chi_i^w}{dx}\frac{d^2\phi_j^w}{dx^2} & \mathrm{E}(x)\frac{d\chi_i^w}{dx}\frac{d^2\phi_j^\theta}{dx^2} \\ \mathrm{E}(x)\frac{d\chi_i^\theta}{dx}\frac{d^2\phi_j^w}{dx^2} & \mathrm{E}(x)\frac{d\chi_i^\theta}{dx}\frac{d^2\phi_j^\theta}{dx^2} \end{bmatrix}_{\Gamma_1}$$

$$\left(k_p\right)_{ij} = \begin{bmatrix} \int_\Omega \left(\chi_i^w\frac{d^2\phi_j^w}{dx^2}\right)d\Omega & \int_\Omega \left(\chi_i^w\frac{d^2\phi_j^\theta}{dx^2}\right)d\Omega \\ \int_\Omega \left(\chi_i^\theta\frac{d^2\phi_j^w}{dx^2}\right)d\Omega & \int_\Omega \left(\chi_i^\theta\frac{d^2\phi_j^\theta}{dx^2}\right)d\Omega \end{bmatrix} \tag{21}$$

where χ_i^w and χ_i^θ are components of the test function, and ϕ_j^w and ϕ_j^θ are the shape functions. The buckling load and its associated modes of buckling are determined by calculating the Eigenvalues and Eigenvectors of Equation (17).

4. Radial basis function (RBF)

By using the RBF, the lateral displacement function of the column '*W*' over the support domain of an arbitrary point can be estimated in terms of its nodal values at all points located in the support domain [45,46]:

$$\begin{aligned} W^h &= \sum_{j=1}^{n} R_j(x)a_j + \sum_{j=1}^{n} S_j(x)b_j = [R]^{\mathrm{T}}\{c\} \\ [R]^{\mathrm{T}} &= \{R_1 \quad S_1 \quad R_2 \quad S_2 \quad \mathrm{L} \quad R_n \quad S_n\} \\ \{c\}^{\mathrm{T}} &= \{a_1 \quad b_1 \quad a_2 \quad b_2 \quad \mathrm{L} \quad a_n \quad b_n\} \end{aligned} \tag{22}$$

where *n* is the number of nodes located in the support domain of the point of interest, W^h is the approximate lateral displacement function, $R_j(x)$ and $S_j(x)$ are the radial basis functions and their derivatives, a_j and b_j are the constant coefficients.

$$S_j(x) = \frac{dR_j(x)}{dx} \tag{23}$$

Using Equation (22) the approximation of rotation can be written as

$$\theta^h = \sum_{j=1}^{n}\frac{dR_j(x)}{dx}a_j + \sum_{j=1}^{n}\frac{dS_j(x)}{dx}b_j \tag{24}$$

Equations (22) and (24) can be written in the following matrix form:

$$\begin{Bmatrix} W \\ \theta \end{Bmatrix}^h = \begin{bmatrix} R_1(x) & S_1(x) & R_2(x) & S_2(x) & \mathrm{L} & R_n(x) & S_n(x) \\ \frac{dR_1(x)}{dx} & \frac{dS_1(x)}{dx} & \frac{dR_2(x)}{dx} & \frac{dS_2(x)}{dx} & \mathrm{L} & \frac{dR_n(x)}{dx} & \frac{dS_n(x)}{dx} \end{bmatrix}\begin{Bmatrix} a_1 \\ b_1 \\ a_2 \\ b_2 \\ \mathrm{M} \\ a_n \\ b_n \end{Bmatrix} = [R]^{\mathrm{T}}\{c\} \tag{25}$$

The constant coefficients vector of Equation (25) can be determined by satisfying this equation in all nodes placed in the support domain [45,46].

$$\{d\} = \left[R_Q\right]\{c\} \tag{26}$$

where $\{d\}$ is a vector that collects the nodal values of lateral displacements and rotations at all nodes located in the support domain and $\left[R_Q\right]$ is the moment matrix defined as follows

$$\left[R_Q\right]=\begin{bmatrix} R_1(x_1) & S_1(x_1) & R_2(x_1) & S_2(x_1) & L & R_n(x_1) & S_n(x_1) \\ \frac{dR_1(x_1)}{dx} & \frac{dS_1(x_1)}{dx} & \frac{dS_1(x_1)}{dx} & \frac{dS_2(x_1)}{dx} & L & \frac{dR_n(x_1)}{dx} & \frac{dS_n(x_1)}{dx} \\ R_1(x_2) & S_1(x_2) & R_2(x_2) & S_2(x_2) & L & R_n(x_2) & S_n(x_2) \\ \frac{dR_1(x_2)}{dx} & \frac{dS_1(x_2)}{dx} & \frac{dR_2(x_2)}{dx} & \frac{dS_2(x_2)}{dx} & L & \frac{dR_n(x_2)}{dx} & \frac{dS_n(x_2)}{dx} \\ M & M & M & M & O & M & M \\ R_1(x_n) & S_1(x_n) & R_2(x_n) & S_2(x_n) & L & R_n(x_n) & S_n(x_n) \\ \frac{dR_1(x_n)}{dx} & \frac{dS_1(x_n)}{dx} & \frac{dR_2(x_n)}{dx} & \frac{dS_2(x_n)}{dx} & L & \frac{dR_n(x_n)}{dx} & \frac{dS_n(x_n)}{dx} \end{bmatrix} \quad (27)$$

Various radial basis functions have been proposed in the literature. The four most often used forms of radial functions are listed in Table 2. In this paper, the thin plat spline (TPS) radial basis function with the shape parameter $\eta=3$ is used. Based on Equation (26), if the moment matrix is nonsingular, there is a unique solution for vector of coefficients.

$$\{c\}=\left[R_Q\right]^{-1}\{d\} \quad (28)$$

By substituting the last equation in Equation (22), The matrix of radial basis function $\left[\phi\right]$ can be obtained as follows.

$$W^h=\left(\left[R\right]^T\left[R_Q\right]^{-1}\right)d=\left[\phi\right]\{d\}$$

$$\left[\phi\right]=\left[R\right]^T\left[R_Q\right]^{-1}= \quad (29)$$
$$\begin{bmatrix}\phi_1^w & \phi_1^\theta & \phi_2^w & \phi_2^\theta & L & \phi_n^w & \phi_n^\theta\end{bmatrix}$$

5. The essential boundary conditions

The RBF possesses the Kronecker delta function property. Hence, in the proposed meshless method, the imposition of displacement boundary conditions can be conducted by a simple procedure such as penalty method. In penalty method, a penalty factor, which is a very large number, is assigned to the diagonal element of the stiffness matrix related to the closed degree of freedom (DOF). Therefore, the displacement of the Intended node must be infinitesimal to have a limited value when a very large number multiplies it. Thus, zero-value displacement at the closed DOF is imposed. It should be noted that if the shape functions do not satisfy the Kronecker delta property, the essential boundary conditions cannot be directly imposed. Up to now, several techniques such as the Lagrange multiplier method have been proposed to resolve this problem. The use of these methods is not convenient since it mainly increases the dimensions of the problem matrices.

6. Numerical results

6.1 Validation

In order to verify the proposed method, results obtained from analysis of a homogenous column by the MLPG method with different node numbers are compared with those obtained from the exact solution. To achieve a homogeneous column in the proposed method, it is enough to assume that the volume fraction exponent takes a big value such as ($\alpha = 1000$) in Equations. (1) to (4). Thus, V_{CNT} becomes zero and it means the column is made of a fully isotropic polymer. It worth mentioning that the exact buckling load of the simply supported homogenous column is obtained using Euler's method.

$$p_{ex}=\frac{\pi^2 E_m I}{L^2}=7.7378\times10^5 \quad (30)$$

In the following, the non-dimensional form of buckling load is used for comparison purposes which is defined as follows:

$$\overline{P}_{cr}=\frac{P_{cr}\times L^2}{E_m\times I_0} \quad (31)$$

Figure 4 illustrates the curve of dimensionless buckling load versus the number of nodes. As can be seen, an increase in the number of nodes causes the results to close the corresponding exact value so that the convergence is achieved in 20 nodes. Table 3 demonstrates the percentage error of the proposed method for different number of nodes. The percentage error in this table is calculated by the following equation.

$$Err\,(\%)=\left|\frac{P_{MLPG}-P_{ex}}{P_{ex}}\right|\times100 \quad (32)$$

Regarding the results of this table, it is found that the MLPG method with ten nodes yields to accurate results (error of less than 0.5%) in the buckling analysis of the column.

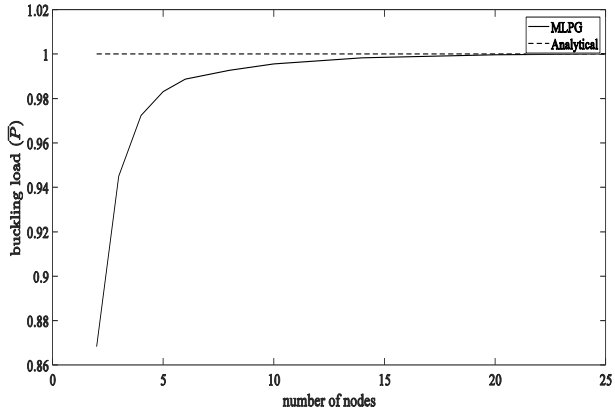

Fig. 4: Effect of number of nodes on buckling load of column.

Table 3: Proper numbers of nodes in the meshless method

Number of nodes	$\overline{P}_{cr}$	Percentage error
2	0.8683	13.17
4	0.9724	2.76
6	0.9887	1.13
10	0.9955	0.44
14	0.9983	0.17
20	0.9996	0.04
25	1.0001	0.01

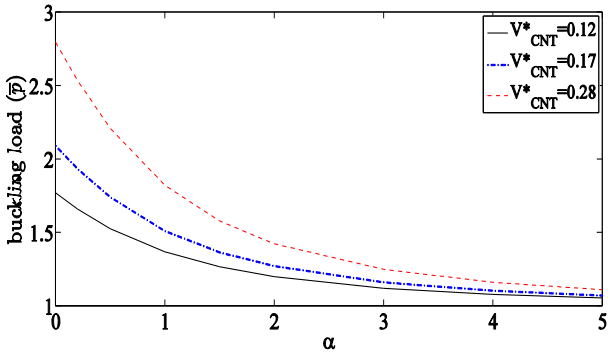

Fig. 5: Effect of CNTs volume fraction exponent α on the buckling capacity of the column (Type 1 and 2 distribution functions)

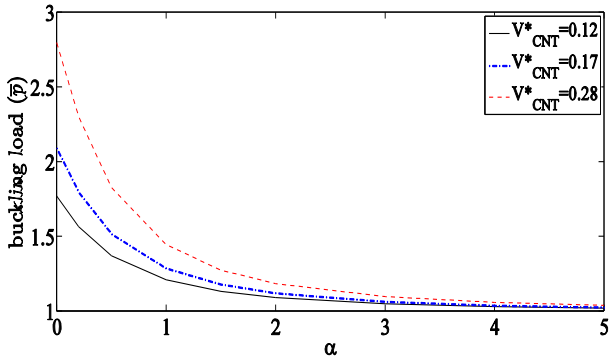

Fig. 6: Effect of CNTs volume fraction exponent α on the buckling capacity of the column (Type 3 distribution function)

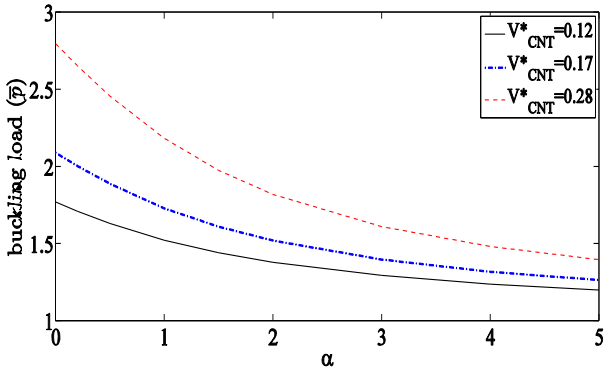

Fig. 7: Effect of CNTs volume fraction exponent α on the buckling capacity of the column (Type 4 distribution function)

6.2 Evaluating the effect of CNTs distribution on the Buckling capacity of column

Figure 5 demonstrates the effect of the CNTs volume fraction exponent α on the buckling capacity of the simply supported column for types 1 and 2 with various V^*_{CNT}. Similar curves are also presented for types 3 and 4 in Figures 6 and 7, respectively. As can be seen, the buckling capacity of the column decreases by increasing the volume fraction exponent, and increases by increasing V^*_{CNT}. Also, the effect of increasing α on the buckling capacity is insignificant for α values higher than 4. The comparison of Figures (5) to (7) reveals that type 3 is of the highest and type 4 is of the lowest sensitivity to volume fraction index α. For Type 4, an increase in the CNTs volume fraction (V^*_{CNT}) has no effect on the buckling capacity at relatively high values of α. It is to be pointed out that there is good agreement between the results obtained by type 1 and 2 functions, which can be justified considering the symmetric ends of the column.

The variation of the buckling load against different values of the CNTs volume fraction exponent for all distribution functions is plotted in Figure 8 for $V^*_{CNT} = 0.12$. As can be seen, the maximum buckling load for all values of α is obtained in type 4, in which the CNTs volume fraction is higher around the mid-height of the column. For type 3 with the highest content of CNTs near the support regions, the lowest buckling load is obtained at all different volume fraction exponents.

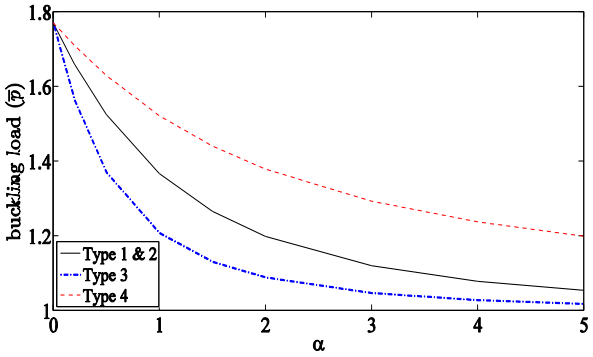

Fig. 8: Comparison of the buckling loads of reinforced columns with different distribution functions for $V^*_{CNT} = 0.12$.

In Figures 9 and 10, the variation of buckling load with CNTs volume fraction exponent for type 3, and various boundary conditions respectively for braced and unbraced columns are presented. In these figures, the letters C, F, and S indicate the clamped, free, and simply supported edges, respectively. According to these figures, the braced C-C end support show the highest sensitivity and the C-F end support shows the least sensitivity to α changes.

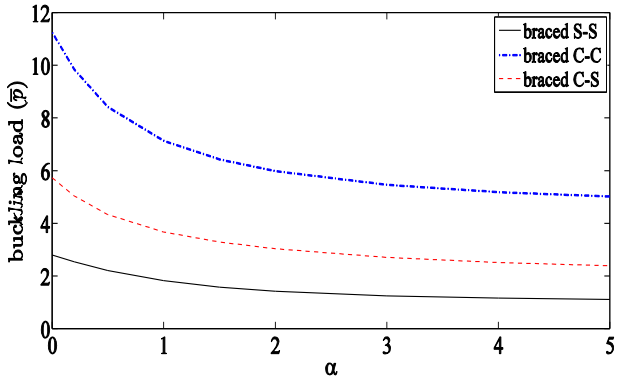

Fig. 9: Effect of CNTs volume fraction exponent variation on buckling capacity of braced columns with Type 3 and $V_{CNT}^{*} = 0.28$ for various end supports.

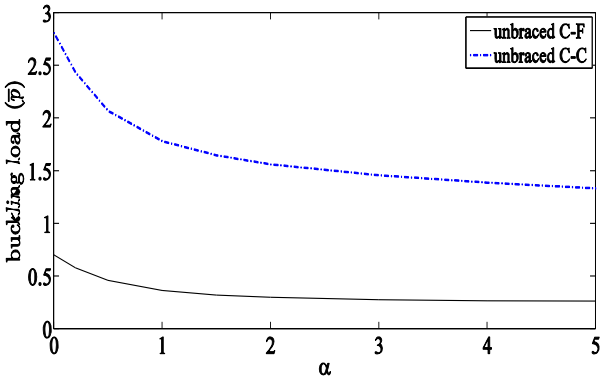

Fig. 10: Effect of CNTs volume fraction exponent variation on buckling capacity of unbraced columns with Type 3 and $V_{CNT}^{*} = 0.28$ for various end supports.

Table 4: A summary of results obtained from buckling analysis of CNT-reinforced columns

	Type 1 and 2 functions				Type 3 function				Type 4 function			
$\boldsymbol{\alpha}$	0.5	1.0	2.0	5.0	0.5	1.0	2.0	5.0	0.5	1.0	2.0	5.0
$\boldsymbol{V_{CNT}^{*} = 0.12}$	1.47	1.36	1.26	1.17	1.37	1.21	1.09	1.02	1.63	1.52	1.38	1.20
$\boldsymbol{V_{CNT}^{*} = 0.17}$	1.66	1.49	1.36	1.22	1.52	1.29	1.12	1.03	1.89	1.73	1.52	1.27
$\boldsymbol{V_{CNT}^{*} = 0.28}$	2.06	1.77	1.56	1.33	1.83	1.44	1.18	1.04	2.46	2.18	1.82	1.40

6.3 Evaluating the efficiency of MLPG method comparing with the finite element method

In this section, to show the efficiency of MLPG method in buckling analysis of FG-CNT reinforced columns, the percentage error of FEM and MLPG methods are compared for type 1 and $V_{CNT}^{*} = 0.12$. Figure 11 shows the error percentage of the FEM method against the number of elements (two node linear beam elements), and Figure 12 shows the error percentage of the MLPG method against the number of nodes. According to these figures, to achieve a proper accuracy (error less than 1%) in the FEM method more than 40 elements are required, and in the MLPG method just 22 nodes are needed. It should be mentioned in these figures, the results of FEM with very fine meshing is considered as the exact solution.

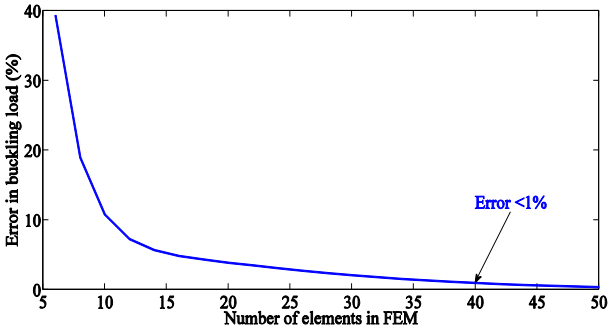

Fig. 11: The effect of the number of elements on the error in buckling load of the FG-CNT reinforced columns with Type 1 and $V_{CNT}^{*} = 0.12$ in FEM.

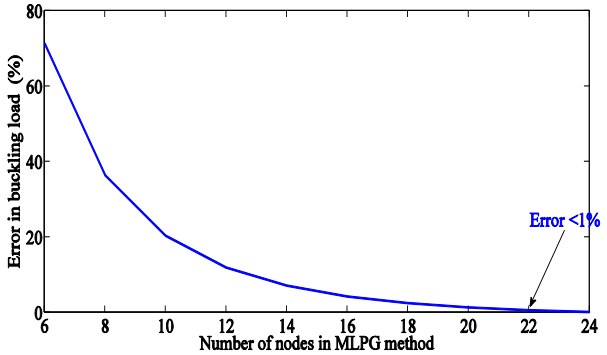

Fig. 12: The effect of the number of nodes on the error in buckling load of the FG-CNT reinforced columns with Type 1 and $V_{CNT}^{*} = 0.12$ in MLPG method.

7. Discussion and conclusion

The present paper has investigated the effect of reinforcing columns by CNTs with different distribution functions on their buckling capacity. Due to functionally graded variations of CNTs volume fraction in the column length, the mechanical properties of the functionally graded material have been modeled by employing the extended rule of mixture.

The MLPG method with RBF interpolation has been utilized for buckling analysis of FGM columns. Results obtained from the buckling analysis of a homogenous column using the proposed method and different numbers of nodes have been validated by comparing them with the

analytical results. Finally, some numerical examples have been solved to examine the effects of different parameters such as the distribution function, volume fraction exponent, and the CNTs volume fraction on the buckling capacity of the column. The most critical remarks are concluded as follows:

- MLPG method with more than ten nodes has sufficient accuracy (error of less than 0.5%) for buckling analysis of columns.
- By increasing the volume fraction exponent, the buckling capacity of the column decreases, and it increases by increasing the CNTs volume fractions.
- Results obtained by type 1 and 2 distribution functions are compatible for simply supported columns at both ends because of symmetric conditions.
- The effect of increasing the volume fraction exponent on the buckling capacity is mitigated at higher values of this parameter.
- For Type 4 distribution function, an increase in the CNTs volume fraction practically has no impact on the buckling capacity at relatively high values of the volume fraction exponent.
- For the simply supported column at both ends, the column reinforcement by a higher volume fraction of CNTs around the mid-height of the column is more effective in enhancing the buckling capacity of the column. In other words, type 4 and 3 distribution functions are the best and worst patterns of the reinforcement for the simply supported column, respectively.

The future research fields for the buckling analysis of AFG CNT reinforced columns are suggested as follows:

- Buckling analysis of reinforced columns with general elastic supports and non-standard support conditions.
- Buckling analysis of columns embedded in an elastic medium.
- Stochastic buckling analysis of columns considering uncertainties in material properties, boundary conditions and loading.
- Buckling analysis of columns under a combined loading such as axial compression and torsion.
- Reinforcing the columns with other nanomaterials such as graphene platelets.
- Investigating the effects of parameters affecting the mechanical properties of nanoparticle reinforced matrices such as agglomeration, poor dispersion of nanoparticle in polymeric or metallic matrix, as well as the weak bonding at the interface between nanoparticle on buckling capacity of columns.

Conflicts of interest

The authors declare that there is no conflict of interest.

References

[1] Chen, W. F., and Lui, E. M., "Structural stability; theory and implementation", Elsevier, New York, 1987.

[2] Timoshenko, S. P., and Gere, J. M., "Theory of elastic stability", Courier Corporation, United States, 2009.

[3] Fiedler, B., Gojny, F.H., Wichmann, M.H.G., Nolte, M.C.M., and Schulte, K., "Fundamental aspects of nano-reinforced composites", Composites Science and Technology, 2006, Vol. 66, pp. 3115-3125.

[4] Rahai, A.R., and Kazemi, S., "Buckling analysis of non-prismatic columns based on modified vibration modes", Communications in Nonlinear Science and Numerical Simulation, Vol. 13, No. 8, 2008, pp. 1721-1735.

[5] Wang, C. M., and Wang C. Y., "Exact solutions for buckling of structural members". CRC press, 2004.

[6] O'Rourke, M., and Zebrowski, T., "Buckling load for nonuniform columns", Computers & Structures, Vol. 7, No. 6, 1977, pp. 717-720.

[7] Dube, G.P., and Dumir, P.C., "Tapered thin open section beams on elastic foundation -I. Buckling analysis", Computers & structures, Vol. 61, No. 5, 1996, pp. 845-857.

[8] Sapountzakis, E. J., and Tsiatas, G. C., "Elastic flexural buckling analysis of composite beams of variable cross-section by BEM", Engineering Structures, Vol. 29, No. 5, 2007,pp. 675-681.

[9] Elfelsoufi, Z., and Azrar, L., "Buckling, flutter and vibration analyses of beams by integral equation formulations", Computers & Structures, Vol. 83, No. 31-32, 2005, pp. 2623-2649.

[10] Huang, Y., and Li, X.F., "Buckling analysis of nonuniform and axially graded columns with varying flexural rigidity", Journal of engineering mechanics, Vol. 137, No. 1, 2011, pp. 73-81.

[11] Bazeos, N., and Karabalis, D.L., "Efficient computation of buckling loads for plane steel frames with tapered members", Engineering Structures, Vol. 28, No. 5, 2006, pp. 771-775.

[12] Soltani, M., Asgarian, B., and Mohri, F., "Improved finite element model for lateral stability analysis of axially functionally graded nonprismatic I-beams", International Journal of Structural Stability and Dynamics, Vol. 19, No. 9, 2019, pp. 1950108.

[13] Liu, G.R., and Gu, Y.T., "An introduction to meshfree methods and their programming", Springer Science & Business Media, Netherlands, 2005.

[14] Heidargheitaghi, F., Ghadiri Rad, M.H., and Kazemi, M., "Buckling Analysis of Non-Prismatic Columns Subjected to Non-Uniform Loading Using the Meshless Local Petrov-Galerkin Method". Computational Methods in Engineering, Vol. 40, No. 2, 2022, pp.39-56.

[15] Soltani, M., "Flexural-torsional stability of sandwich tapered I-beams with a functionally graded porous core", Journal of Numerical Methods in Civil Engineering, Vol. 4, No. 3, 2020, pp. 8-20.

[16] Soltani, M., and Asgarian, B., "Finite element formulation for linear stability analysis of axially functionally graded nonprismatic timoshenko beam", International Journal of Structural Stability and dynamics, Vol. 19, No. 2, 2019, p.1950002.

[17] Soltani, M., Asgarian, B., and Jafarzadeh, F., "Finite difference method for buckling analysis of tapered Timoshenko beam made of functionally graded material", AUT Journal of Civil Engineering, Vol. 4, No. 1, 2020, pp.91-102.

[18] Soltani, M., "Finite Element Modeling for Buckling Analysis of Tapered Axially Functionally Graded Timoshenko Beam on Elastic Foundation", Mechanics of Advanced Composite Structures, Vol. 7, No. 2, 2020, pp.203-218.

[19] Soltani, M., and Asgarian, B., "Exact stiffness matrices for lateral–torsional buckling of doubly symmetric tapered beams with axially varying material properties", Iranian Journal of Science and Technology, Transactions of Civil Engineering, Vol. 45, No. 2, 2021, pp.589-609.

[20] Soltani, M., Atoufi, F., Mohri, F., Dimitri, R., and Tornabene, F., "Nonlocal elasticity theory for lateral stability analysis of tapered thin-walled nanobeams with axially varying materials", Thin-Walled Structures, Vol. 159, 2021, p.107268.

[21] Soltani, M., Atoufi, F., Mohri, F., Dimitri, R., and Tornabene, F., "Nonlocal Analysis of the Flexural–Torsional Stability for FG Tapered Thin-Walled Beam Columns", Nanomaterials, Vol. 11, No. 8, 2021, p.1936.

[22] Rad, M.H.G., Shahabian, F., and Hosseini, S.M., "Geometrically nonlinear dynamic analysis of FG graphene platelets-reinforced nanocomposite cylinder: MLPG method based on a modified nonlinear micromechanical model", Steel and Composite Structures, Vol. 35, No. 1, 2020, pp. 77-92.

[23] Lee, C., Wei, X., Kysar, J.W., and Hone, J., "Measurement of the elastic properties and intrinsic strength of monolayer graphene", science, Vol. 321, No. 5887, 2008, pp. 385-388.

[24] Kazemi, M., Rad, M.H.G., and Hosseini, S.M., "Nonlinear dynamic analysis of FG carbon nanotube/epoxy nanocomposite cylinder with large strains assuming particle/matrix interphase using MLPG method", Engineering Analysis with Boundary Elements, Vol. 132, 2021, pp.126-145.

[25] Sudak, L., "Column buckling of multiwalled carbon nanotubes using nonlocal continuum mechanics", Journal of applied physics, Vol. 94, No. 11, 2003, pp. 7281-7287.

[26] Goudah, G., Suliman, S.M.A., and Elfaki, E.A., "Carbon Nanotubes and Their Composites: A Review", Sudan Eng. Society Journals, Vol. 58, No. 1, 2019.

[27] Zhang, W., Suhr, J., and Koratkar, N.A., "Observation of high buckling stability in carbon nanotube polymer composites", Advanced Materials, Vol. 18, No. 4, 2006, pp. 452-456.

[28] Han, Y., and Elliott, J., "Molecular dynamics simulations of the elastic properties of polymer/carbon nanotube composites", Computational Materials Science, Vol. 39, No. 2, 2006, pp. 315-323.

[29] Yas, M., and N. Samadi, "Free vibrations and buckling analysis of carbon nanotube-reinforced composite Timoshenko beams on elastic foundation", International Journal of Pressure Vessels and Piping, Vol. 98, 2012, pp. 119-128.

[30] Lei, Z.X., Liew, K.M., and Yu, J.L., "Free vibration analysis of functionally graded carbon nanotube-reinforced composite plates using the element-free kp-Ritz method in thermal environment", Composite Structures, Vol. 106, 2013, pp. 128-138.

[31] Li, Q., Liu, J., and Xu, S., "Progress in research on carbon nanotubes reinforced cementitious composites", Advances in Materials Science and Engineering, 2015.

[32] Mirzaei, M., and Kiani, Y., "Free vibration of functionally graded carbon nanotube reinforced composite cylindrical panels", Composite Structures, Vol. 142, 2016, pp. 45-56.

[33] Arani, A.J., and Kolahchi, R., "Buckling analysis of embedded concrete columns armed with carbon nanotubes", Computers and Concrete, Vol. 17, No. 5, 2016, pp. 567-578.

[34] Wang, Q., Qin, B., Shi, D., and Liang, Q., "A semi-analytical method for vibration analysis of functionally graded carbon nanotube reinforced composite doubly-curved panels and shells of revolution", Composite Structures, Vol. 174, 2017, pp. 87-109.

[35] Karami, B., Janghorban, M., Shahsavari, D., Dimitri, R., and Tornabene, F., "Nonlocal buckling analysis of composite curved beams reinforced with functionally graded carbon nanotubes", Molecules, Vol. 24, No. 15, 2019, p. 2750.

[36] Civalek, O., and Jalaei, M.H., "Shear buckling analysis of functionally graded (FG) carbon nanotube reinforced skew plates with different boundary conditions", Aerospace Science and Technology, Vol. 99, 2020, p. 105753.

[37] Liew, K.M., Lei, Z.X., and Zhang, L.W., "Mechanical analysis of functionally graded carbon nanotube reinforced composites: a review", Composite Structures, Vol. 120, 2015, pp. 90-97.

[38] Ghayoumizadeh, H., Shahabian, F., and Hosseini, S.M., "Elastic wave propagation in a functionally graded nanocomposite reinforced by carbon nanotubes employing meshless local integral equations (LIEs)", Engineering Analysis with Boundary Elements, Vol. 37, No. 11, 2013, pp. 1524-1531.

[39] Ghoohestani, S., Shahabian Moghadam, F., and Hosseini, S.M., "Dynamic analysis of a layered cylinder reinforced by functionally graded carbon nanotubes distributions subjected to shock loading using MLPG method", Computer Modeling in Engineering and Sciences-CMES, Vol. 100, No. 4, 2014, pp. 295-321.

[40] Rad, M.H.G., Shahabian, F., and Hosseini, S.M., "Geometrically nonlinear elastodynamic analysis of hyper-elastic neo-Hooken FG cylinder subjected to shock loading using MLPG

method", Engineering Analysis with Boundary Elements, Vol. 50, 2015, pp. 83-96.

[41] Hosseini, S.M., and Zhang, C., "Elastodynamic and wave propagation analysis in a FG graphene platelets-reinforced nanocomposite cylinder using a modified nonlinear micromechanical model", Steel and Composite Structures, Vol. 27, No. 3, 2018, pp. 255-271.

[42] Hosseini, S.M., and Zhang, C., "Coupled thermoelastic analysis of an FG multilayer graphene platelets-reinforced nanocomposite cylinder using meshless GFD method: A modified micromechanical model", Engineering Analysis with Boundary Elements, Vol. 88, 2018, pp. 80-92.

[43] Nguyen, T.N., Thai, C.H., Luu, A.T., Nguyen-Xuan, H., and Lee, J., "NURBS-based postbuckling analysis of functionally graded carbon nanotube-reinforced composite shells", Computer Methods in Applied Mechanics and Engineering, Vol. 347, 2019, pp. 983-1003.

[44] Zhou, T., and Song, Y., "Three-dimensional nonlinear bending analysis of FG-CNTs reinforced composite plates using the element-free Galerkin method based on the SR decomposition theorem", Composite Structures, Vol. 207, 2019, pp. 519-530.

[45] Rad, M.H.G., Shahabian, F., and Hosseini, S.M., "A meshless local Petrov–Galerkin method for nonlinear dynamic analyses of hyper-elastic FG thick hollow cylinder with Rayleigh damping", Acta Mechanica, Vol. 226, No. 5, 2015, pp. 1497-1513.

[46] Raju, I.S., Phillips, D.R., and Krishnamurthy, T., "A radial basis function approach in the meshless local Petrov-Galerkin method for Euler-Bernoulli beam problems", Computational Mechanics, Vol. 34, No. 6, 2004, pp. 464-474.

[47] Raju, I.S., and Phillips, D.R., "Further developments in the MLPG method for beam problems", Computer Modeling in Engineering and Sciences, Vol. 4, No. 1, 2003, pp.141-160.